Cellular convection in a chamber with a warm surface raft

J. A. Whitehead,[1,a)] Erin Shea,[2] and Mark D. Behn[3]
[1]*Physical Oceanography, Woods Hole Oceanographic Institution, MS#21, WHOI Woods Hole, Massachusetts 02543, USA*
[2]*EAPS, Massachusetts Institute of Technology, Cambridge, Massachusetts 02139, USA*
[3]*Geology and Geophysics, Woods Hole Oceanographic Institution, Massachusetts 02543, USA*

(Received 2 May 2011; accepted 13 September 2011; published online 20 October 2011)

We calculate velocity and temperature fields for Rayleigh-Benard convection in a chamber with a warm raft that floats along the top surface for Rayleigh number up to $Ra = 20\,000$. Two-dimensional, infinite Prandtl number, Boussinesq approximation equations are numerically advanced in time from a motionless state in a chamber of length L' and depth D'. We consider cases with an insulated raft and a raft of fixed temperature. Either oscillatory or stationary flow exists. In the case with an insulated raft over a fluid, there are only three parameters that govern the system: Rayleigh number (Ra), scaled chamber length ($L = L'/D'$), and scaled raft width (W). For $W = 0$ and $L = 1$, linear theory shows that the marginal state without a raft is at a Rayleigh number of $2^3\pi^4 = 779.3$, but we find that for the smallest W (determined by numerical grid size) the raft approaches the center monotonically in time for $Ra < 790$. For $790 < Ra < 811$, the raft has a decaying oscillation consisting of raft movement back and forth accompanied by convection cell reversal. For $811 < Ra < 871$, the oscillation amplitude is constant in time and it increases with larger Ra. Finally, there is no raft motion for $Ra > 871$. For larger raft widths, there is a range of W that produces raft oscillation at each Ra up to 20 000. Rafts in longer cavities ($L = 2$ and 4) have almost no oscillatory behavior. With a raft of temperature set to different values of T_r rather than insulating, a fixed Rayleigh number $Ra = 20000$, a square chamber ($L = 1$), fixed raft width, and with internal heat generation, there are two ranges of oscillating flow. © *2011 American Institute of Physics*. [doi:10.1063/1.3651341]

I. INTRODUCTION

The dynamics of Rayleigh-Benard convection form an important conceptual framework for the understanding of stability and transition of fluid flows. It is not surprising that, being a nonlinear problem, the dynamics takes on new features with the introduction of additional processes of even minuscule size. Double diffusion is an excellent example of such new behavior; a minute gradient of a second substance with different diffusivity than temperature can lead to completely new stability behavior for buoyancy driven flow.[1] However, the new process need not occur in the interior, as is the case with double diffusion—rather a change along the boundaries can also lead to new behavior as long as, apparently, the change introduces a nonlinear process. Examples of such processes include: experiments and theory for heaters floating near the top of fluid that develop a spontaneous drift;[2] floating rafts of thermally insulating material that move laterally by modulating the convection cells beneath them in experiments with water heated from below;[3] cyclical motion of clusters of balls on the flat bottom of an experimental convection cell heated from below in more viscous liquid;[4] and the interaction between Earth's surface continents and mantle convection as illustrated in numerical models developed by the geophysics community.[5] Dynamic models of these processes[6] indicate a strong feedback between a laterally mobile insulator and the underlying pattern of convection.

These studies indicate that a numerical study of floating rafts on top of convection cells spanning a wide range of the driving parameters would complement both the laboratory and more applied geophysical modeling studies, which generally have been studied over only a limited range of parameters. For example, a systematic documentation of behavior for cellular convection with a raft from the critical value of Rayleigh number, Ra, upward has never been performed. Here, we present such a first-order study in an attempt to explore this parameter space.

We investigate models of convection with the utmost simplicity using idealized rafts. Specifically, we investigate (1) what values of Ra, raft width, and chamber lengths produce moving rafts, (2) the conditions under which the presence of a raft affects flow, and (3) what chamber sizes result in vigorous raft motions and what sizes do not?

To answer such questions, we numerically calculate the time evolution of temperature, fluid flow, and raft location in a convection model driven by elevated temperature ΔT along the bottom of a chamber of constant depth. The calculations start from zero velocity and constant cold interior temperature. The utmost simplicity is desired; hence, we study two-dimensional flow in Cartesian coordinates. We use the Boussinesq approximation, which assumes that every fluid property is constant except for thermal expansion acting in the buoyancy term of the equations. We consider free slip

a)Author to whom correspondence should be addressed. Electronic mail: jwhitehead@whoi.edu. Tel.: 508-289-2793. Fax: 508 289 4181.

boundaries everywhere and examine the case for an infinite Prandtl number Pr fluid (so that inertial terms in the momentum equations are dropped). Over 500 calculations are performed spanning Ra up to 20 000, a range of raft widths, three different cavity lengths, and some cases with internal heat generation, h, within the fluid.

Two different types of temperature boundary conditions are considered for the surface raft. The first type (Section III) is a thermally insulating raft. It is probably the most primitive configuration because the only dimensionless numbers are the Rayleigh number Ra, internal heating h, and two geometric variables: the ratio of raft width to chamber width W and the ratio of the chamber length to depth L (for clarity, we say that the chamber always has a length and the raft always has a width). The second type (Section IV) uses a raft of fixed temperature T_r. Results span a range from cellular convection with minimum effects from the raft ($T_r \ll 1$) to forced stratified flow for a very hot raft ($T_r > 1$). To retain the utmost simplicity, the raft exerts no drag forces on the underlying fluid. The raft is simply moved at the velocity of fluid at its center unless the raft is being pressed against the side in which case the raft velocity is set to zero. In both types of raft temperature boundary conditions, the free-slip stress condition is unchanged. Therefore, the rafts only alter the temperature or heat flow condition at the top. In this sense, the raft is as rudimentary as possible.

In spite of this simplicity, the raft has an enormous influence on convection for some parameters, but only a minor influence for others. The largest influence results from a raft that moves back and forth periodically causing the convection cell to perpetually reorganize. The reorganization consists of the periodic growth and decay of two cells with opposite circulation, a motion that is not present without the raft for all the ranges of Ra and L. The minor influence occurs when the raft is held fixed by the convection cells at some location such that it determines the phases of the cells and to some extent the exact magnitude of the flow. There are three such locations for trapping a stationary raft: the raft can be held to the side by a steady convection cell, the raft can be held steadily over the convergence point above a sinking region, or the raft can be held steadily over the divergence point of an upwelling region.

II. FORMULATION OF THE PROBLEM

A. Governing dynamics

The basic equations for this model in Cartesian coordinates express continuity, momentum conservation, and energy conservation:

$$\nabla' \cdot \tilde{u}' = 0, \tag{1a}$$

$$\rho \frac{\partial \tilde{u}'}{\partial t'} + \rho(\tilde{u}' \cdot \nabla')\tilde{u}' == -\nabla' p' + \nabla' \cdot \tilde{\tilde{\tau}}' + g\alpha\rho_0 T' \hat{k}, \tag{1b}$$

$$\frac{\partial T'}{\partial t'} + \tilde{u}' \cdot \nabla' T' = \kappa \nabla'^2 T' + \frac{H'}{\rho C_p}, \tag{1c}$$

in which the velocity vector is $\tilde{u}'$, density is ρ with the average density ρ_0, temperature is T', time is t', the stress tensor is $\tau'_{ij} = \mu\left(\frac{\partial u'_i}{\partial x'_j} + \frac{\partial u'_j}{\partial x'_i}\right)$, viscosity is constant and denoted by μ, acceleration of gravity is g, the linear thermal coefficient of expansion is α, thermal diffusivity is κ, internal heat generation is H', specific heat at constant pressure is C_p, and $\hat{k}$ is a unit vector in the direction of gravity directed downward in the z' coordinate direction. The prime denotes dimensional variables (temperature, velocity, time, and location); dimensionless variables have the prime omitted. Initially the temperature everywhere is T'_0. The fluid is in a two-dimensional chamber of depth D'. Temperature is the same along the top except under the raft, and the temperature of a strip centered along the bottom is suddenly raised to $T'_0 + \Delta T'$ at a time that we set to zero.

The variables are made dimensionless using a velocity scale κ/D', temperature scale $\Delta T'$, time scale D'^2/κ, and internal heating scale $\rho C_p \kappa \Delta T'/D'^2$, where $\kappa = k/\rho_0 C_p$. Henceforth, dimensionless (unprimed) variables are used. Dimensionless temperature is $T = \left(T' - T'_0\right)/\Delta T'$.

The heat equation is

$$\frac{\partial T}{\partial t} + \tilde{u} \cdot \nabla T = \nabla^2 T + h. \tag{2a}$$

For two-dimensional Cartesian flow with the origin at the lower left of the chamber and positive directions into the chamber, the equation for vorticity $\zeta = \partial w/\partial x - \partial u/\partial z$ is

$$\nabla^2 \zeta = -Ra \frac{\partial T}{\partial x}, \tag{2b}$$

and the equation for the stream function ψ where $u = -\partial\psi/\partial z$ and $w = \partial\psi/\partial x$ is

$$\nabla^2 \psi = \zeta. \tag{2c}$$

The Rayleigh number is $Ra = g\alpha\Delta T D^3/\kappa\nu$ in which $\nu = \mu/\rho_0$. Equation (2a) is advanced numerically using a leapfrog-trapezoidal scheme for each time step δt. Then, Eq. (2b) is solved by inverting the Poisson equation, after which Eq. (2c) is solved using the same Poisson equation inversion scheme. Boundary conditions are set to $\psi = \zeta = 0$ on all boundaries. At the top boundary, $T = 0$ except for locations where the raft is present, in which case either the heat flow is zero ($\partial T/\partial z = 0$) or the surface temperature is fixed to a given value, T_r. The bottom boundary has $T = 1$, and the sides have zero heat flux, so that $\partial T/\partial x = 0$. The initial conditions are $\psi = \zeta = T = 0$ in the interior.

The raft speed is set equal to the speed of the flow at the center of the raft. Therefore, for a raft whose center is located at c, the raft is moved according to $dc/dt = u(c, 0)$. In order to view only the thermal consequences of having a raft at the top of the fluid, there is free slip between the fluid and the raft. One can think of the raft as being slightly elevated above the fluid surface, but insulating it thermally and having a "keel" or "drogue" at its center that connects it to the fluid.

The benefit of investigating such a simple problem is that calculations are efficiently made and numerous runs can be performed rapidly covering a wide range of the governing parameters. In addition to Ra, the only additional

dimensionless numbers needed to describe the problem are internal heating h, chamber length $L = L'/D'$, and raft width W, which is scaled by the chamber length so that $W = W'/L'$. Calculations cover the range of $500 \leq Ra \leq 20000$ and raft widths range from smallest possible (which depends on the numerical grid size) to the largest possible, which is $W = 1$. Four grid sizes (16, 32, 64, and 128) were originally tested, but the 32 grid was found to be sufficient for evaluating results over wide ranges of the governing parameters, balancing calculation speed, and model resolution. The calculations consistently show that grid size has no effect of the qualitative nature of the results so that regime diagrams are unchanged, although the exact location of the boundaries between regimes is calculated more precisely with finer grid resolution. Naturally such a regular grid creates some special behavior. For example, any combination of flow field, temperature field, and raft location that is perfectly symmetrical in the horizontal direction about the midpoint of the chamber at the beginning of a model run remains that way forever. Thus, any raft starting at the center with symmetric initial flow and temperature (including of course zero values) remains there forever.

B. Calibration

To calibrate this system, convection with only bottom heating and no raft present is numerically calculated in the range $500 < Ra < 900$. We find that our benchmark results are identical to the analytical results for convection with the same parameters. With a square chamber cross section ($L = 1$), linear theory shows that convection at the value $Ra = 2^3\pi^4 = 779.2727$ is neutrally stable. Numerical runs were started with a linear initial temperature distribution and a perturbation to violate the symmetry mentioned above. This perturbation is simply one off-center interior grid point set to a temperature of 1. That perturbation immediately initiates a small forced flow, and by 35 numerical time steps, the signal spreads throughout the numerical grid. The maximum value of the stream function is found to be decaying in time for $Ra = 779$ (for all time steps thereafter) but growing in time at 780.

III. CONVECTION WITH AN INSULATING RAFT

A. Chamber with $L = 1$

We first show results for the simplest possible configuration—a square chamber ($L = 1$) with no internal heating ($h = 0$) and an insulating raft with smallest width W. Based on results for ordinary convection without a raft, the results for the 32 square chamber are adequately resolved in all aspects, and we continue to use this grid size hereafter. For the width of the raft, the smallest value of $W = 1/32$ occupies only one grid point, which is not desirable because a float occupying one grid point cannot be located at the exact center of the top boundary. Consequently, it does not allow a steady flow underneath it with perfect left-right symmetry. Instead, we choose the raft width $W = 1/16 = 0.0625$, so that a left-right symmetric flow can develop if the raft stops at the center. In this case, the only independent variable is Ra, and for a fixed value of Ra, the velocity and temperature are calculated over time along with the raft position.

We start by observing the response of the system to the presence of the raft for $Ra < 812$. There are many possible dependent variables that illustrate the results of such a calculation: maximum value of vorticity, maximum value of heat flux, or raft location come to mind. However, because our primary focus is on the moveable raft, it is useful to first examine the trajectories of raft location with time. For small Ra, the raft gradually went to the center and stopped. For example, with $Ra = 500$, the approach of the center of the raft to the center of the top is monotonic and is dominated by two features that may be due to the discrete size of the grid (Figure 1(a)). First, there are two changes in the slope of the

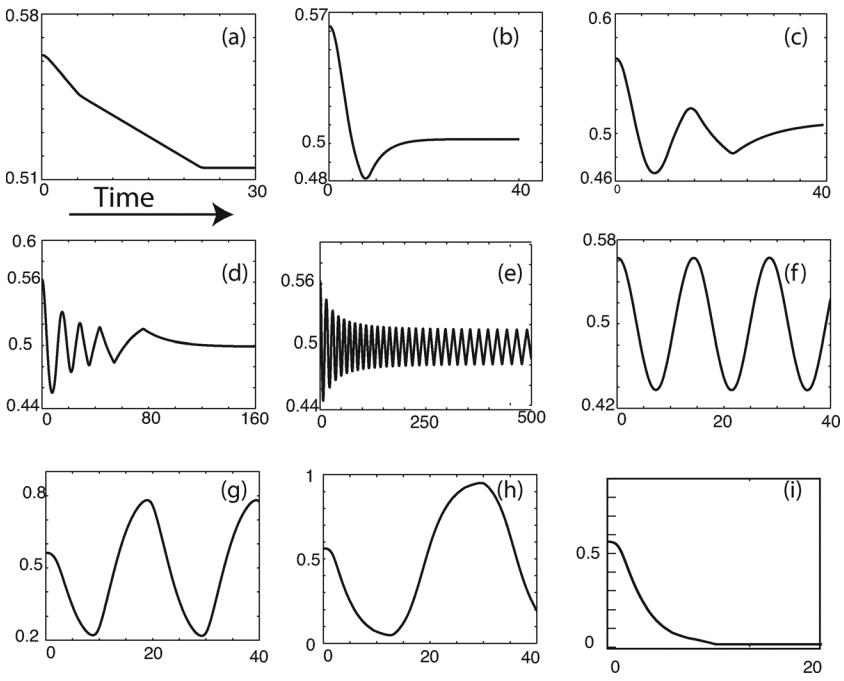

FIG. 1. Trajectories of the raft with time for a raft width $W = 0.0625$. The vertical axis the location of the center of the raft and the lateral axis is time. The values of Ra are (a) 700, (b) 800, (c) 807, (d) 810, (e) 812, (f) 815, (g) 845, (h) 870, and (i) 872.5.

position versus time at times of about 6 and 23 as the center of the float encounters large changes in velocity as it moves from grid point to grid point. Second, the raft coordinate does not approach exactly 0.5 because the numerical scheme places the raft at a specific grid location set by the rounded-off value of the raft location coordinate. Once the raft is numerically set on a grid location, if velocity at that location goes to zero the raft location coordinate stops changing. Although these effects are relatively easy to see in this case, such significant effects from the finite grid size are not noticeable at larger *Ra*.

The critical Rayleigh number (above which we find steady oscillations) is in the range $811 < Rac < 812$. Approximately 1% below *Rac*, the raft overshoots the center after which its trajectory decays (Figure 1(b)), and closer to *Rac*, there are decaying oscillations (Figures 1(c) and 1(d)). The exact ranges of overshoot and decaying oscillations are unknown.

For values above *Rac*, only one cell forms and it continually moves the raft to one side. Once the raft is there, the insulation from the raft warms the fluid below it, and a new cell of opposite sign grows under the raft and expels the previous cell. Therefore, the raft oscillates back and forth (Figures 1(e)–1(h)). For the smallest value of *Ra* in this range, the excursion has a peak to peak amplitude of only one numerical grid point (panel e), and for larger *Ra*, the amplitude increases (Figure 2). Near *Rac*, the increase of amplitude with *Ra* is close to vertical. Then, for values of *Ra* from about 815 progressing up to approximately 850, the increase appears to be close to linear and from there to 860 there is a bit of curvature. At approximately 860, the increase in amplitude with *Ra* changes back to a linear relationship but with a different slope, possibly signifying raft interaction with the sides of the tank. Finally, at $Ra = 871$, the oscillating behavior vanishes. Instead, the raft is swept to the side of the tank by the convection cell where, for $872 \leq Ra \leq 20,000$, it is pinned by a steady flow (Figure 1(i)). The raft ends up on either the left or the right side of the tank, depending on whether the raft was right or left of center (respectively) at the start of the calculation. The initial upwelling is on the same side of center as the raft, and because only one cell emerges above *Rac*, the cell sweeps the raft to the side opposite to the initial upwelling.

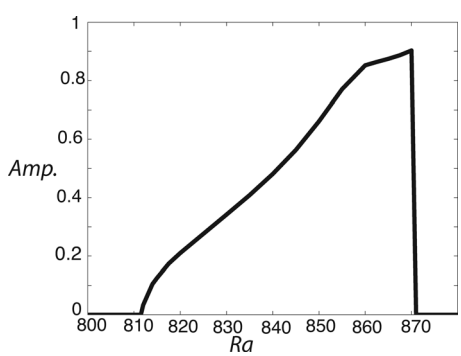

FIG. 2. Amplitude of oscillation as a function of *Ra* for a raft with width $W = 0.0625$.

The streamlines and temperature contours for various flows illustrate the raft-flow interaction. For $Ra < 812$, where there is no oscillatory flow, a typical numerical run begins with the raft placed off center. Soon, one convection cell forms with upwelling on the side occupied by the raft. This cell moves the raft toward the center. As the raft approaches the center, a flow with two cells is seen to emerge in addition to the single cell. The second cell is seen first in the top corner behind the moving raft and it rapidly grows so that the upwelling stagnation point soon overtakes the raft. Then, the raft becomes centered in the middle and upwelling occurs under it, with sinking on both sides of the chamber. Once the raft arrives at the exact center of the top of the chamber, where the lateral velocity is zero, the single cell vanishes and the raft remains fixed over the double cell (Figure 3).

Since the raft lies at the diverging point on the top of the upwelling with two cells, it is reasonable to expect that the raft position might be unstable since a small displacement to one side or the other would sweep the raft onto a flow away from the center. This does not occur in this parameter range because a displacement of the raft quickly produces the single cell seen in the transient case. This single cell is superimposed on the two cells, and it produces velocity in a direction to drive the straying raft back toward the center.

The mechanism driving the oscillation for $Ra > Rac$ simply involves the same single eddy (Figure 4). In this case, the raft moves to one side and soon the insulating properties cause a warm thermal signal to diffuse down into the cold sinking region. The region becomes warmed and the cell changes direction. The new cell drives the raft back toward the other side. The flow is rapid enough to allow the raft to overshoot the center before the new reversed thermal signal develops.

Next, flows are calculated over time for other values of *W* in chambers with $L = 1$. The characteristics of flows that are found after a long time are illustrated with a regime diagram in *Ra*-*W* space in Figure 5. Either a periodic oscillation

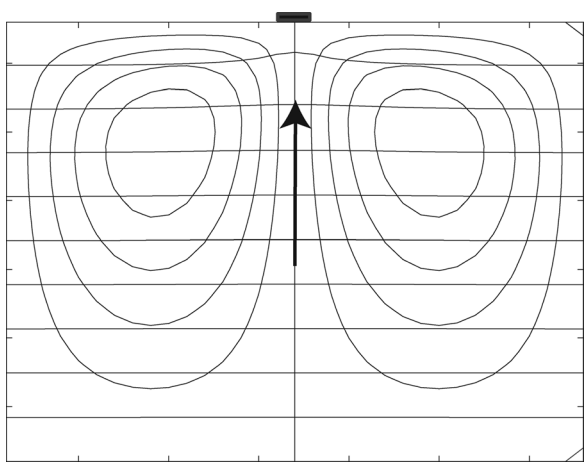

FIG. 3. The steady subcritical flow for $W = 0.0625$ and $Ra = 700$ at $t = 30$. An insulating raft (black block) has been drawn to the center and remains there indefinitely. The stream function (closed contours) reveals two cells. The steady state temperature contours (every 0.1) are almost perfectly horizontal (black lines).

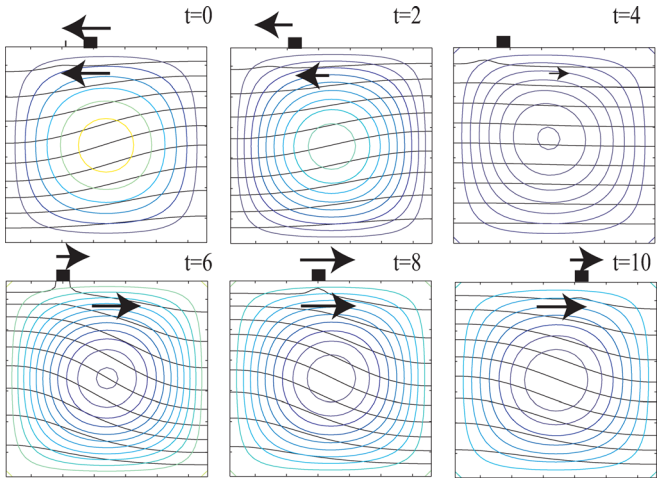

FIG. 4. (Color online) Sections of temperature (black contours, every 0.1) and velocity (color or gray contours) every two time units during half an oscillation cycle for an insulating raft with Ra = 850 and $W = 0.0625$. The black block at the top illustrates the location of the raft. The arrows show the flow directions of the raft and of the fluid immediately below the raft.

of the raft position, with the amplitude of back and forth oscillation (full scale excursion) shown by the number, or a stationary flow is found. The oscillatory flow is always symmetric about the center of the chamber so all flows follow a sequence identical to the example in Figure 4. The stationary flow has two modes: In one, the raft is swept to the sinking side of the convection cell and then held there by the convergence of the surface flow. There is only one convection cell in the chamber. This mode is found for W smaller than the width to produce oscillations and below the lower dashed line in Figure 5; denoted by "D." The second stationary mode has the raft held at the center over an upwelling with two cells and sinking along each sidewall as shown by Figure 3 for subcritical Ra. It is denoted by "U" and is found for W larger than the width to produce oscillations. The region is above and to the left of the top dashed line in Figure 5.

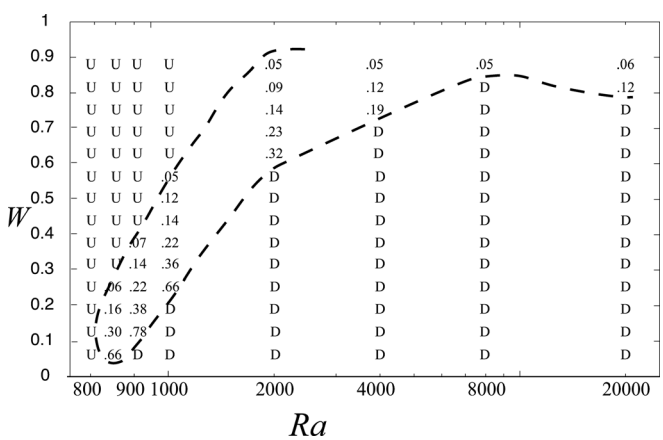

FIG. 5. Regime diagram for an insulating raft with $L = 1$. Oscillatory flow is found inside the dashed area with the number denoting the full amplitude of the excursion back and forth. Symbols are U—stationary raft centered over steady upwelling and D—stationary raft held to the side over a steady sinking region.

B. Chamber with $L = 2$ or 4

Convection in a chamber with $L = 2$ (a 32×64 chamber) has almost no tendency for the raft to oscillate, but otherwise it has similar results to the square chamber (Figure 6). There are two observed oscillations. The first oscillation is found exactly at $Ra = 8000$ and $W = 0.75$, where a large raft moves back and forth opening sinking regions on alternating sides. For flow at $Ra = 7000$, and also to the left and above the dashed line, the raft is stationary and centered over an upwelling. For flow at $Ra = 9000$ and to the right and below the dashed line, the raft is stationary and held to the side of the tank. The second oscillation is not shown in Figure 6 because it was found in between the grid points in a narrow region of Ra-W space near 800 and 0.05. A full exploration of both regions is not completed yet. In three widths at $Ra = 20\,000$, the flow is irregular with time. In these cases, transient thermals descend from the top unstable boundary layer at irregular times. This irregular flow is described in more detail in Section V B.

The convection in a chamber with aspect ratio 4 ($L = 4$) (128 lateral grid points) has only steady flow in Ra-W space (Figure 7). As with the lower aspect ratio flows, the raft is held fixed over a sinking region for smaller W and over an upwelling region for larger W. In some cases, it takes considerable time, much greater than one time unit, to come to steady flow as the three or four cells in the chamber sort themselves out in the presence of the raft. For the case of a raft over a sinking region, the cells show two arrangements (Figures 8(a) and 8(b)); either the raft is trapped at the boundary with three cells present (most commonly, and at lower Ra) or the raft is trapped over the center of two cells with sinking at the center. The latter is only found at larger Ra and then only if the raft is placed near the center or if the raft arrives at the center as the cells evolve. There seems to be hysteresis between the three and two cell arrangements for a given value of W, but no detailed study is completed. With the raft over an upwelling region, the cells also show two arrangements; either there are two unequal cells

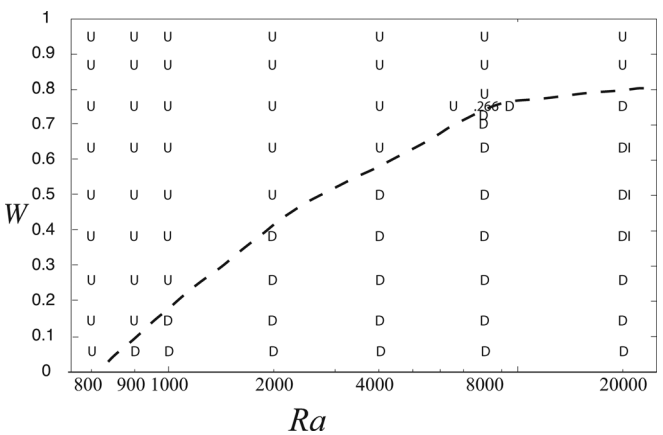

FIG. 6. Regime diagram for an insulating raft with chamber aspect ratio $L = 2$. One set of parameters ($Ra = 8000$, $W = 0.75$) on this grid produced an oscillation whose amplitude is shown by the number. Symbols are U—stationary raft centered over steady upwelling, D—stationary raft held to the side over a steady sinking region, and DI—stationary raft held to the side over an irregular and unsteady sinking region.

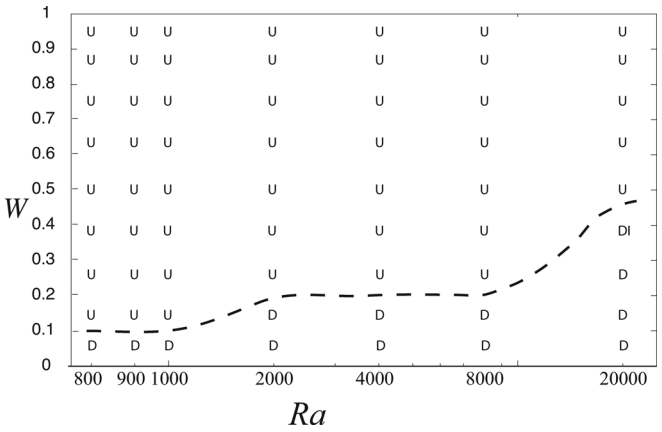

FIG. 7. Regime diagram for an insulating raft with a cell aspect ratio of $L=4$. Symbols are U—raft over steady upwelling, D—raft over a steady sinking region, and DI—raft held to the side over an unsteady sinking region.

(Figure 8(c)), with upwelling under a raft that is separated from the boundary by one cell (for smaller *Ra*), or there are two equal cells (Figure 8(d)) with the raft centered over the upwelling, with consequent sinking at the boundary (for larger *Ra*). Upwelling never traps a raft at the boundary. There appears to be no sign of hysteresis between these two arrangements, but further study is warranted. Because the hysteresis question remains open, Figure 7 contains no information of the number of cells in *Ra*-*W* space.

In summary, the oscillations are only found for the case of $L=1$ except for one case with $L=2$. Generally, the raft is trapped at a sinking location for small rafts and at an upwelling location for large ones.

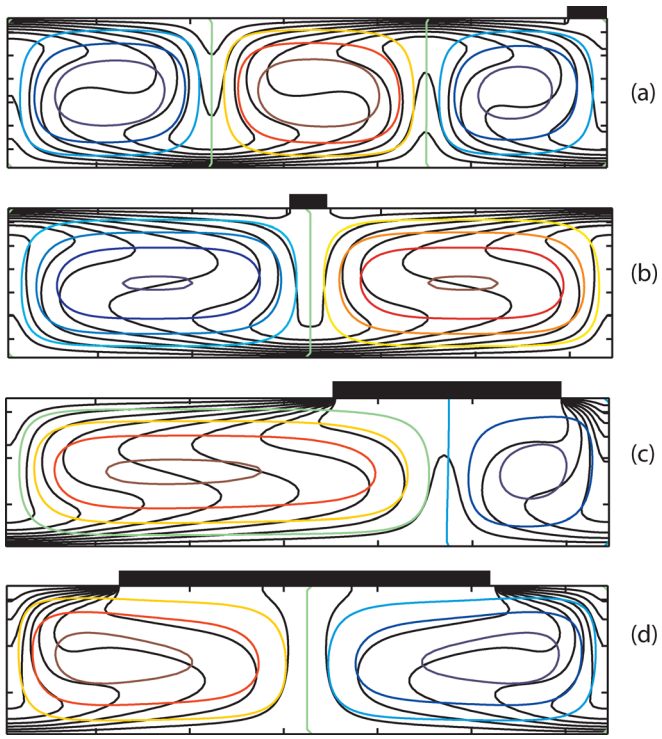

FIG. 8. (Color online) Sections of temperature (black contours, every 0.1) and velocity (gray contours) for the four arrangements of cells and raft for $L=4$.

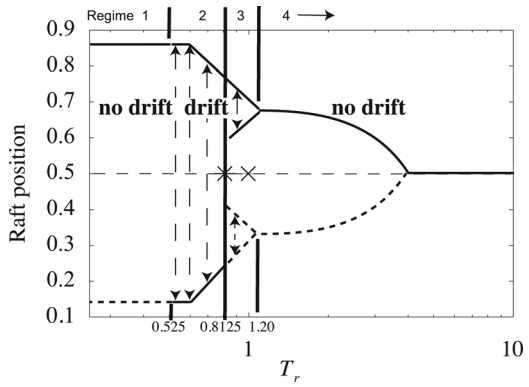

FIG. 9. Regimes of flow for the raft of fixed temperature at Ra = 20 000 as a function of T_r. In the vertically dashed regions with arrowheads (Regimes 2 and 3), the raft moves back and forth. In Regimes 1 and 4, the raft becomes stationary at the location shown by the solid (or, by reflection symmetry, dotted) lines. Because of reflection symmetry about the centerline of the chamber, a stationary raft can be trapped in either one of the two locations unless it is at the exact center. A perfectly symmetric flow with the raft at the exact center is shown by the light dashed line. This flow is unstable to small perturbations of raft position off the center except for the two points designated by ×, where stationary flow emerges even though the raft is initially started slightly off center.

IV. A RAFT WITH A SPECIFIED TEMPERATURE, THREE VARIABLES

A. *Ra* = 20 000

If the temperature of the raft is specified as T_r, then there is one additional parameter driving the system as compared with the system in Section III with an insulating raft. If internal heating (h) is also applied, there is a second additional parameter. With these modifications, the drifting behavior of the raft extends to higher values of *Ra*. The results for numerous runs varying T_r at $Ra=20\,000$, $W=0.25$, $L=1$, and $h=8$ are typical of this system and are, therefore, shown in detail here. There are four regimes of flow (Figures 9 and 10). Regime 1 ($T_r<0.525$) is identical to the "D" mode for $L=1$ in Section III. The raft is swept to the sinking side of the convection cell and then trapped there by the convergence of the surface flow. There is one convection cell in the chamber. Two such states are possible, one with clockwise circulation and with the raft held on the right wall and the other with mirror symmetry to that (dashed line). In Regime 2 ($0.525<T_r<0.8125$, Figure 11), both symmetries of cell flow are realized, but the raft goes back and forth across the top of the chamber and alternately triggers one cell and then the other because the flow direction in the cell abruptly reverses at the end of each traverse. It is identical to the oscillation in Section III for $L=1$. In Regime 3 ($0.8125<T_r<1.2$, Figure 12), two convection cells exist that produce sinking along both sidewalls and rising under the raft. One cell is stronger than the other and the speeds of the two cells become stronger and weaker cyclically. In the extreme limit of this regime, one cell dies away completely and then reemerges. In Regime 4, $T_r\geq 1.2$ the two cells are stationary, but of differing strength. For increasing T_r in this regime, the two cells become closer in strength and the raft location is progressively closer to the center of the cell. Finally, for $T_r>4$,

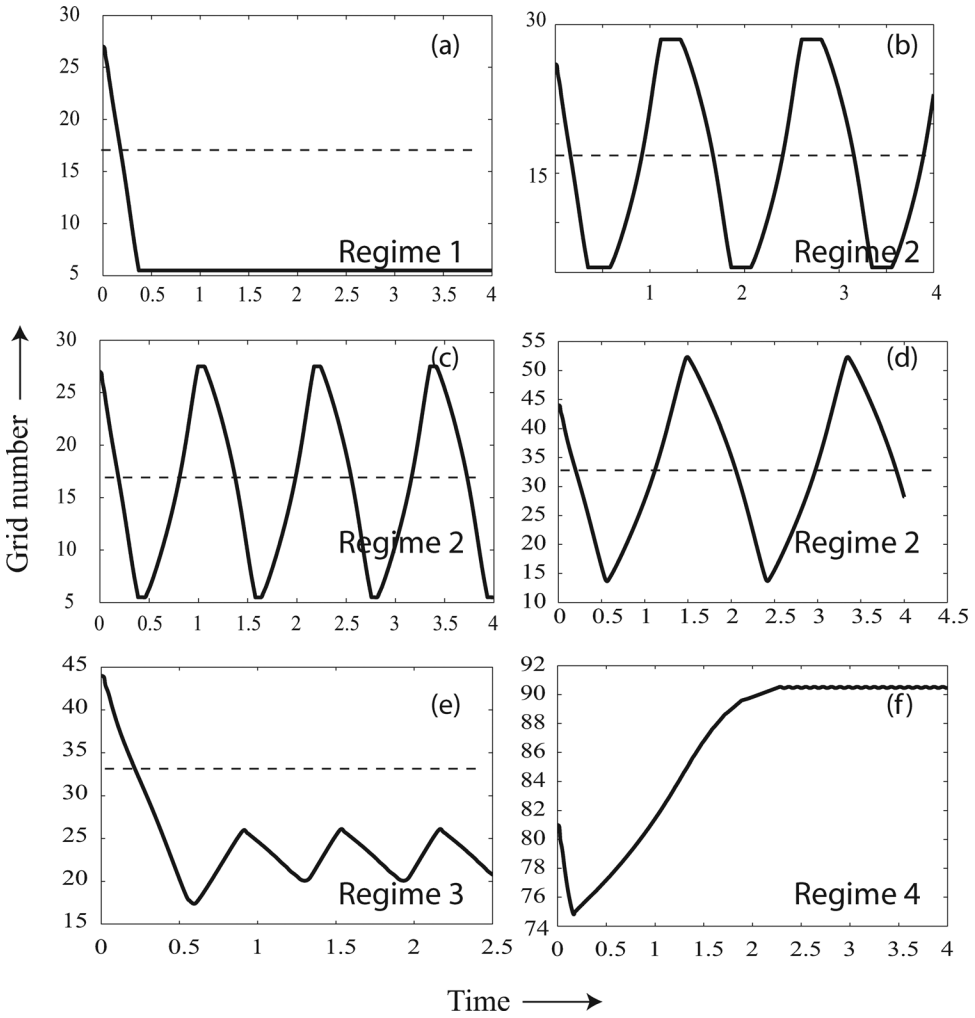

FIG. 10. The trajectories of the raft center for the four regimes with Ra = 20 000 shown in Figure 9. The values of T_r for each panel left to right and then down are (a) 0.52, (b) 0.525, (c) 0.55, (d) 0.7125, (e) 0.9, and (f) 2.0. Grid units are used to show the range of grid sizes used. The dashed line is the center except for Regime 4 with 128 × 128 grid points, where the center is off scale.

the raft is at the center, and we have returned to the primitive two cell flow with a stationary raft over upwelling first shown in Figure 3.

The raft goes to the center and stops over the upwelling fluid for two other parameters as well. One has exactly $T_r = 0.8125$, the precise value of T_r between Regimes 2 and 3. The other is for $T_r = 1$. In both of these cases, numerous calculations with assorted grid sizes and time steps show that the raft is swept to the center and stops. Therefore, a motionless raft surrounded by two cells of equal size is a stable fixed point not only for $1.20 < T_r < 4$, but also for $T_r = 0.8125$ and 1.

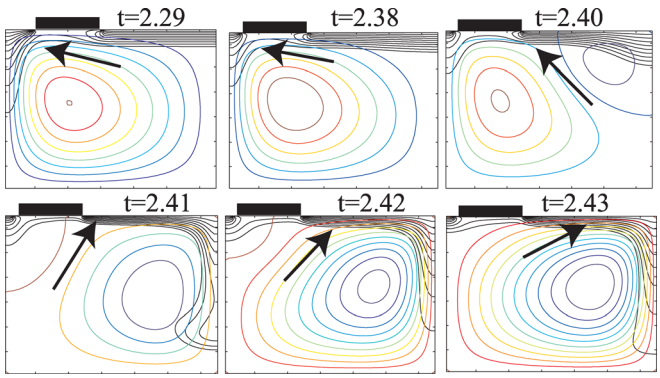

FIG. 11. (Color online) Isotherms (black contours every 0.1), arrows indicating flow direction, and stream function (color or gray contours) in an example of a reversal in flow direction for a Regime 2 oscillation with $T_r = 0.7125$. The descending thermal on the left slowly gets weaker. Then, rather suddenly within 0.02 time units, a new descending thermal develops on the right.

B. *Ra* = 4000

Results of similar calculations for $Ra = 4000$ are shown in Figure 13. There are only three regimes instead of four. The former, time-dependent Regime 3, where the raft is trapped on one side with two cells cyclically alternating in strength is gone. It is possible that this is because the Rayleigh number is too low to have a double cell in the chamber.

V. OTHER NONLINEAR EFFECTS

A. Hysteresis of flow modes

In one case, the calculations give evidence of hysteresis and multiple values for the same driving parameters. It is not clear whether the multiple values arise as a result of the finite-difference scheme and the symmetry of the grid about the middle of the chamber. The Rayleigh number is 20 000, the grid is 64 square, and the raft has a constant temperature

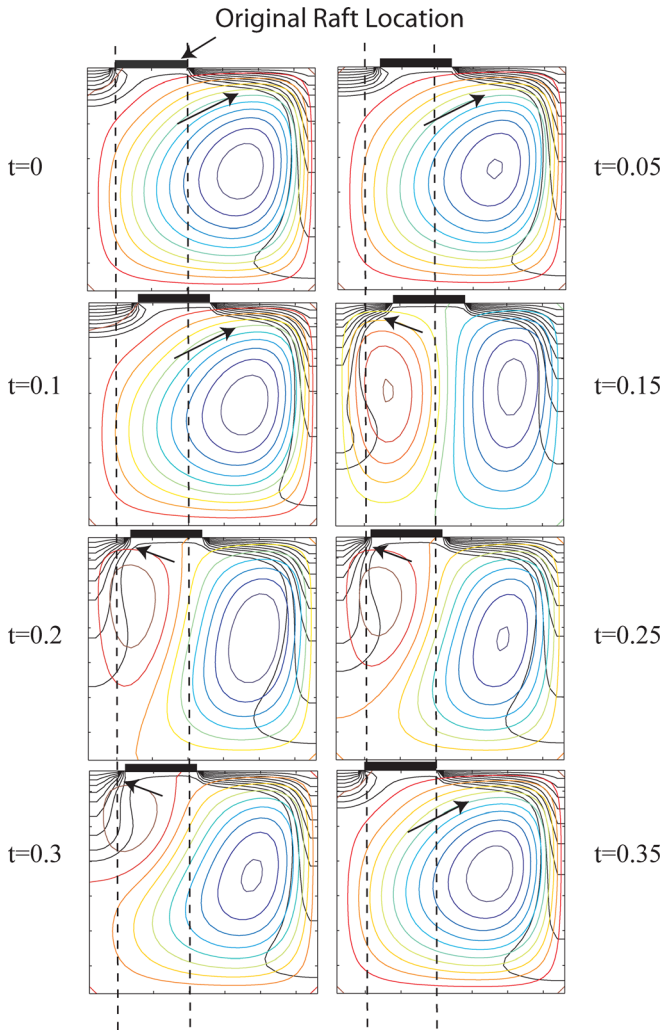

FIG. 12. (Color online) Isotherms (black contours every 0.1), arrows indicating flow direction, and stream function (color or gray contours) in an example of a cycle in a Regime 3 oscillation. The raft goes back and forth synchronously with a circulation cell on the left starting and stopping periodically. The dividing streamline between the two cells moves laterally and this causes the raft (thick block) to move back and forth. The dashed lines show the location of the two edges of the raft at the beginning of this cycle. One arrow in each frame shows flow direction.

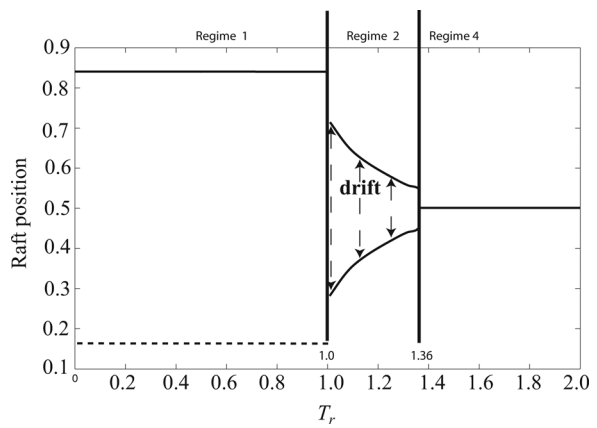

FIG. 13. Regimes of flow for the raft at $Ra = 4000$ as a function of T_r. The regimes behave as the Regimes 1, 2, and 4 shown in Figures 9 and 10.

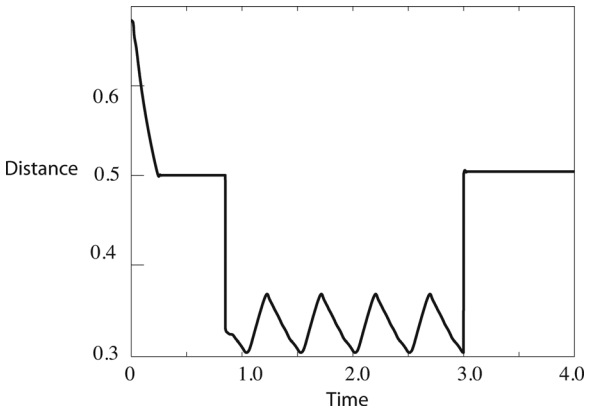

FIG. 14. Raft location over time for a case where the raft becomes initially captured into a right-left symmetric mode above a flow with two cells of equal size. Then, it is artificially moved to a location near the edge and a Regime 3 oscillation develops. When the raft is instantly moved back to the center point at $t = 3$, the symmetric mode develops again even though the temperature distribution is quite non symmetric when it is moved.

$T_c = 1$. Figure 14 shows how the two states are possible, one with oscillations and the other with the raft at the center (denoted by an $\times$ in Figure 9). After starting, the raft moves to the center and is captured there. Then, if the raft location is instantly changed to a value within the range of oscillations indicated in Figure 9, an oscillation will develop. However, if the raft is placed outside the oscillation range, the raft returns to the center. In the example shown in Figure 14, the new location is 0.328, but other locations in the range that gives an oscillation also produce the oscillation cycle. After the oscillation has developed, if the raft is instantly relocated to the center (0.5), the raft starts to drift but the drift decays and the raft becomes stationary at the center after a brief period of drift. The small amount of drift after relocation is just visible in Figure 14. Therefore, there are two flows and both are stable to small disturbances. One is steady and the other is oscillatory.

B. Irregular behavior

Some irregular flows developed. They occur more easily with internal heating, but it is not required since some examples are reported in Section III in which $h = 0$. The example illustrated here (Figure 15) has $L = 2$, $Ra = 20\,000$, and $W = 0.25$, with a raft that is held fixed over the upwelling end. The irregular time series and velocity time series broke out along the thermal boundary layer after a short time.

The mechanism is visible in Figure 16. There is one convection cell with rising on the right under the insulator. The thermal boundary layer stretches across the entire top and the cold fluid sinks along the left wall, but at the same time, it develops a growing bulge that begins to grow into a cold sinking region. The bulge is swept toward the left end as it grows. Usually, it reaches the left end before sinking all the way to the bottom, but occasionally it descends into the interior before reaching the left end. In this case, it temporarily produces two cells in the stream function, but the left cell quickly dies away and one cell remains. This event is repeated at irregular intervals.

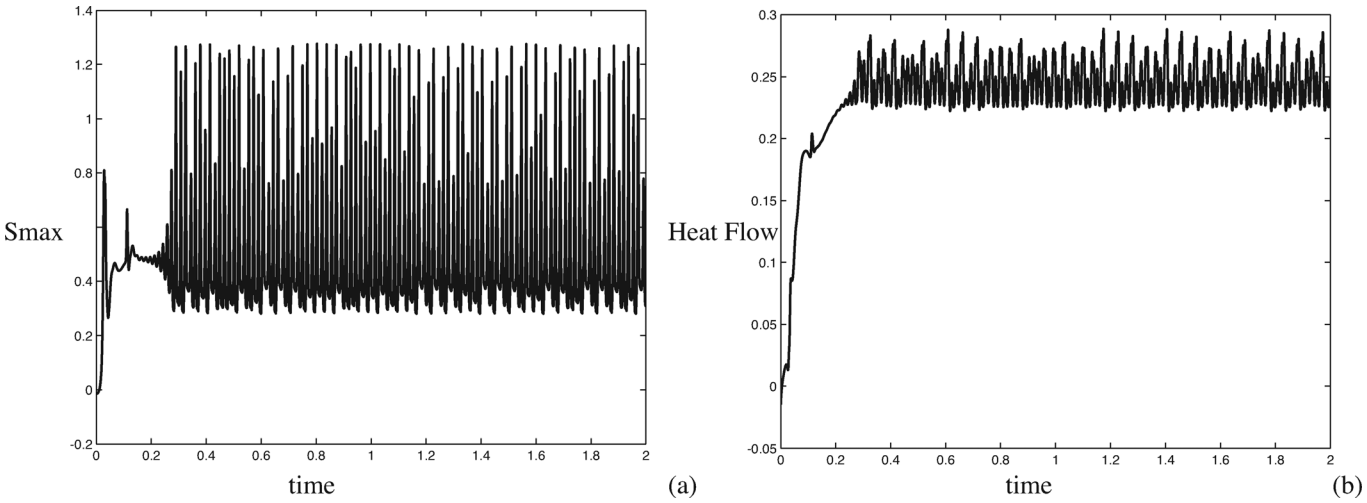

FIG. 15. Time series of irregular flow: (a) maximum value of the stream function and (b) conductive heat flow at the top center of the chamber.

VI. DISCUSSION

We have explored the marginal stability and finite amplitude behavior for convection heated uniformly from below with a small raft that possesses either insulating or fixed temperature conditions. Naturally, the linear instability differs from the standard Rayleigh-Benard problem because a fixed raft produces a small flow at all values of Ra. The instability appears in the form of an oscillation of the raft. Since the raft size is obviously limited by grid size, it is unclear whether an insulated raft in the limit of $W \to 0$ produces oscillations above $Ra = 779$ or not. The stability analysis would have to be expanded as a two-parameter stability analysis around the critical value of Ra. Such an analytical stability analysis has not yet been conducted.

This study indicates that the parameter space for even these very simple cases is rich in different results. The various regions of oscillation are characterized by clear boundaries, although there may be multiple states in a few instances. An irregular and possibly chaotic time series for the convection is found for some examples but only for cases with a stationary raft. For cases in which the raft moves after large time, the flow and raft trajectories are oscillatory.

Clearly the value of L is the most important parameter for determining whether there are oscillations or not. Very close to Rac with $L = 1$, only the lowest lateral wavelength mode is a growing mode for convection without the raft. Thus, the raft directly excites the cell corresponding to this mode, but the flow sweeps the raft to the opposite side of the tank and excites the opposite circulation. A first approximation of this system can be built by starting with the well known amplitude equation for one convection cell that exactly fits in the chamber without a raft of the form $\frac{da}{dt} = (Ra - Rac/Rac)a - a^3$ (Ref. 7) in which a is the amplitude of the convection cell. The value of Rac that must be used pertains to a cell that exactly fits in the box rather than the minimum in the growth rate curve that is usually used for cells in a layer of infinite horizontal extent. Let us take the convention that positive a implies upward flow along the origin (left wall), and thus flow to the right at the top of the chamber. Then, we can add to this equation a term that represents the insulating nature of a raft. The convention will be that b is zero when the raft is exactly in the middle of the tank, since in that case the raft provides extra heat to the fluid exactly at the center of the chamber and it reinforces neither upwelling nor sinking along the left wall. Therefore, we let b be positive when the raft is to the right of center and negative to the left of center, and we subtract a term linearly proportional to b to the amplitude equation. There is an implicit assumption that the raft moves so slowly that the temperature signal from the moving insulator conducts completely into the fluid below the insulator with little alteration from either raft or fluid movement. Finally, the equation for the movement of b is $db/dt = a$. Altogether, the equations for amplitude and raft position are

$$\begin{aligned} \frac{da}{dt} &= \left(\frac{Ra - Rac}{Rac}\right)a - \varepsilon b - \left(a^2\right)a, \\ \frac{db}{dt} &= +a. \end{aligned} \tag{3}$$

The coefficient ε couples the location of the raft with the buoyancy forces from the heat supplied to the fluid from the raft. This coefficient is found by solving a thermal conduction equation and therefore it is proportional to either W for an insulted raft or T_r for a fixed temperature raft in addition to geometric terms. No determination of the exact value of ε is made here; it is set equal to one for the example shown in Figure 17. The equations are easily advanced in time numerically and oscillations result. We find with a number of calculations with fixed Ra that as ε becomes smaller and smaller, the maximum of b during a cycle becomes larger and larger (Figure 17). The value $|b| > 0.5$ is found for some value of the parameters. If $|b| = 0.5$ is imposed numerically at the next time step (to force the raft to remain in the chamber), the oscillation stops. Also, for fixed ε as the value of Ra is increased above Rac, the amplitude of the maximum value of b during a cycle increases in a manner similar to Figure 2.

While the Ra of the Earth's mantle ($\sim 1 \times 10^6$) is significantly larger than that explored in this study, it is useful to

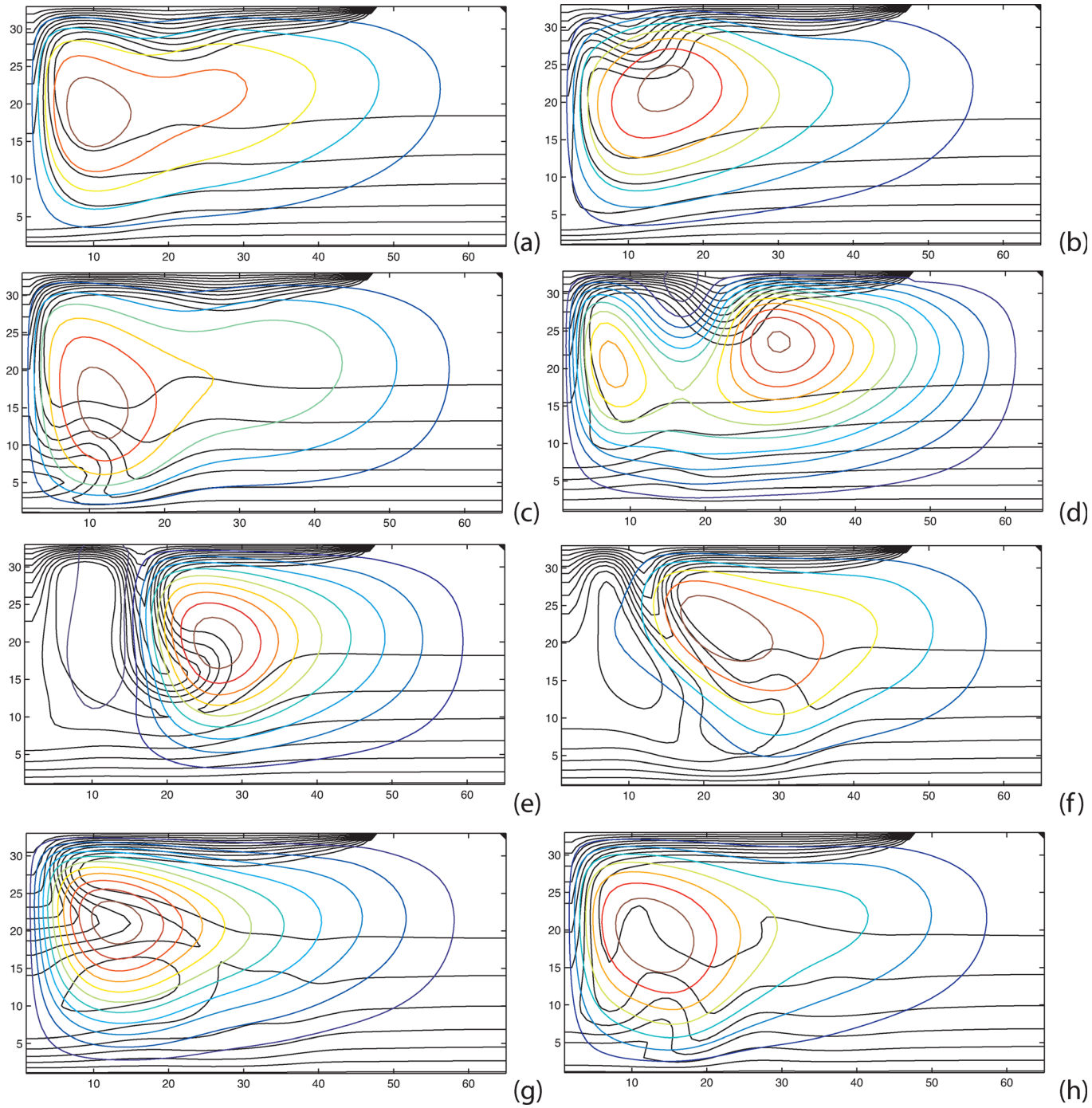

FIG. 16. (Color online) Temperature (black contours) and streamfunction (color or gray contours) for irregular flow at $Ra = 20\,000$ with the raft held fixed along the right side. The sinking boundary layer lies either along the left wall or it descends within the interior at irregular times. Panels are 0.02 time units apart left to right and down with time starting at 1.26

consider our results with respect to plate tectonics—with the rafts acting as rough analogues for the continents riding on top of the mantle. On Earth, the Wilson cycle describes the assembly and breakup of supercontinents over time-scales of multiple hundreds of millions of years. Similar cyclicity is found in our numerical simulations. As stated above, the side boundaries of the chamber in our models are free-slip, allowing us to reflect the cellular pattern across either side boundary. When the continent/raft converges on one side, it can be thought to form a supercontinent with its reflection. When the plate moves away from the edge, the supercontinent breaks up, in a simple example of a Wilson cycle. From this perspective, the insulating effect of rafts (continents) on mantle convection is critical to supercontinent formation and breakup. In this scenario, the continents serving as insulators increase the mantle temperature below and change the dynamics of convection, which in turn affects continent dynamics. The fact that the cycle seems to vanish with increasing Ra is new. It indicates that the penetration of a thermal signal below the raft is greatest when flow is sufficiently slow to

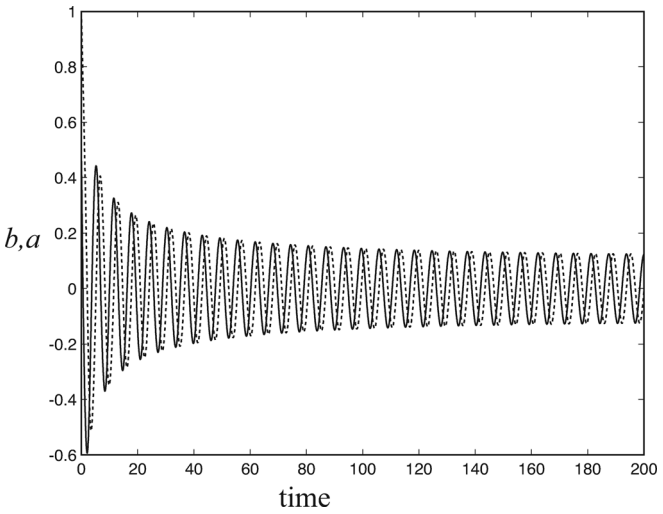

FIG. 17. Solution to the amplitude Equation (3) for $Ra-Rac/Rac=0.01$, $\varepsilon=1$. The solid curve is the amplitude a, and the dots show raft locations b, which lag amplitude slightly in time.

allow the signal to conductively penetrate through a substantial depth of the convection region.

The link between penetration of a thermal signal and flow speed is revealed by the fact that the periods of oscillation in Figures 1, 10, and 14 are of order one and this is true even for $Ra=20\,000$ (Figure 10). Because the order one period is scaled by the thermal diffusion time scale and because that time scale is many tens of billions of years in the Earth's mantle, this seems to rule out the relevance of the oscillations we see here for plate tectonics on Earth. (For a time scale estimate, use $D'=1000$ km and $\kappa=10^{-6}$ m^2 s^{-1} yielding about 30 billion years (Ref. 5) or roughly eight times the age of the Earth.) This agrees with a recent study (Ref. 9) that indicates that a supercontinent primarily modulates mantle convection by determining subduction locations rather than by warming the mantle below it through thermal insulation effects. However, the values of Ra explored in this study ($\sim 10^2-10^4$) are much lower than for the Earth's mantle ($\sim 1\times 10^6$). Perhaps runs at larger Ra will produce cyclic behavior with faster cycles (though there is little evidence for such rapid cyclic behavior at larger Ra in our current models). Thus, based on the results presented here, modulation of deep mantle convection by the insulating effects of continents (to produce, for example, the Wilson cycle) does not seem to be in accord with our primitive model.

VII. CONCLUSION

For insulated rafts, oscillations exist in discrete regions of parameter space and are always symmetric about the center. A range of raft widths have oscillations for $800<Ra<20\,000$ with $L=1$. However, runs with $L=2$ have only two examples of oscillatory behavior in very small parameter ranges, and with $L=4$, there are no oscillations. For a raft of fixed temperature in the range $T_r<0.525$ with $Ra=20\,000$, $L=1$, and $W=0.24$, the raft is swept to one side and remains pinned there by a steady flow. For $0.525\le T_r\le 0.8125$, the raft oscillates about the center and in the range $0.8125<T_r<1.20$, the raft oscillates off center. The oscillation amplitude decreases until finally the raft is stationary at $T_r\ge 1.20$ and offset from the center. For increasing T_r, the offset moves toward the center of the tank and the raft is stationary and centered for $T_r\ge 4$. There are a few points where special flows exist that are different from flows in nearby parameter space.

ACKNOWLEDGMENTS

This project was initiated as a Geodynamics project of the Deep Ocean Exploration Institute at Woods Hole Oceanographic Institution.

[1]J. S. Turner, *Buoyancy Effects in Fluids* (Cambridge University Press, New York, 1973), pp. 251–287.
[2]J. Elder, "Convective Self-propulsion of Continents," Nature **214**, 657 (1967); L. N. Howard, W. V. R. Malkus, and J. A. Whitehead, "Self-convection of rafting heat sources: A model for continental drift," Geophys. Fluid Dyn. **1**, 123 (1970); J. A. Whitehead, "Moving heaters as a model of continental drift," Phys. Earth Planet. Interiors **5**, 199 (1972).
[3]J. Zhang and A. Libchaber, "Periodic boundary motion in thermal turbulence," Phys. Rev. Lett. **84**, 4361 (2000); J.-Q. Zhong and J. Zhang, "Thermal convection with a freely moving top boundary," Phys. Fluids **17**, 115105 (2005); "Dynamical states of a mobile heat blanket on a thermally convecting fluid," Phys. Rev. E **75**, 055301 (2007).
[4]B. Liu and Zhang J. "Self-induced cyclic reorganization of many bodies through thermal convection," Phys Rev Lett. **100**, 244501 (2008).
[5]M. Gurnis, "Large-scale mantle convection and the aggregation and dispersal of supercontinents," Nature **332**, 695 (1988); Zhong and M. Gurnis, "Dynamic Feedback Between a Continentlike Raft and Thermal Convection," J. Geophys. Res. **98**(B7), 12219, doi:10.1029/93JB00193 (1993); J. P. Lowman and G. T. Jarvis, "Mantle convection flow reversals due to continental collisions," Geophys. Res. Lett. **20**, 2087, doi:10.1029/93GL02047 (1993); "Mantle convection models of continental collision and breakup incorporating finite thickness plates," Phys. Earth Planet. Inter. **88**(1), 53 (1995); "Continental collisions in wide aspect ratio and high Rayleigh number two-dimensional mantle convection models, J. Geophys. Res. **101**(B11), 25485, doi: 10.1029/96JB02568 (1996); S. D. King, J. P. Lowman and C. W. Gable, "Episodic tectonic plate reorganizations driven by mantle convection," Earth Planet. Sci. Lett. 203, **83** (2002); D. E. Koglin Jr., S. R. Ghias, S. D. King, G. T. Jarvis, and J. P. Lowman, "Mantle convection with reversing mobile plates: A benchmark study," Geochem., Geophys. Geosyst. **6**, Q09003, doi: 10.1029/2005GC000924 (2005); V. P. Trubitsyn and V. V. Rykov "A 3-D numerical model of the Wilson cycle," J. Geodyn. **20**, 63 (1995); L. Guillou and C. Jaupert, "On the effect of continents on mantle convection," J. Geophys. Res. **100**(B12), 24217, doi: 10.1029/95JB02518 (1995); B. R. Phillips, and H.-P. Bunge, "Supercontinent cycles disrupted by strong mantle plumes," Geology **35**(9), 847 (2007); R. R. Phillips and N. Coltice, "Temperature beneath continents as a function of continental cover and convective wavelength," J. Geophys. Res. **115**, B04408, doi: 10.1029/2009JB006600 (2010); C. A. O'Neill, A. M. Jellinek, and L. Moresi, "Influence of supercontinents on deep mantle flow," Gondwana Res. **15**(3-4), 276 (2009); C. M Cooper, A. Lenardic, and L. Moresi, "The thermal structure of stable continental lithosphere within a dynamic mantle," Earth Planet. Sci. Lett. **222**, 807 (2004); S. M. Honda, M. Yoshida, S. Ootorii, and Y. Iis, "The timescales of plume generation caused by continental aggregation," Earth Planet. Sci. Lett. **176**, 31 (2000); M. Yoshida, Y. Iise, and S. Honda, "Generation of plumes under a localized high viscosity lid in 3-D spherical shell convection," Geophys. Res. Lett. **26**, 947 (1999); A. Lenardic, L. Guillou-Frottier, J-C. Mareschal, C. Jaupart, L. N. Moresi, and W. M. Kaula, "What the mantle sees: The effects of continents on mantle heat flow," Geophys. Monogr. **121**, 95 (2000); Z.-X. Li and S. Zhong, "Supercontinent–superplume coupling, true polar wander and plume mobility: Plate dominance in whole-mantle tectonics," Phys. Earth Planet. Inter. **176**, 143 (2009); A. Lenardic, L. N. Moresi, A. M. Jellinek, and M. Manga, "Continental insulation, mantle cooling, and the surface area of oceans and continents," Earth Planet. Sci. Lett. **134**, 317 (2005); N. Coltice, B. R. Phillips, H. Bertrand, Y. Ricard, and P. Rey, "Global

warming of the mantle at the origin of flood basalts over supercontinents," Geology **35**, 391, (2007); C. Grigne, S. Labrosse, and P. J. Tackley, "Convection under a lid of finite conductivity in wide aspect ratio models: Effect of continents on the wavelength of mantle flow," J. Geophys. Res. **112**, B08403, doi: 10.1029/2006JB004297 (2007); B. R. Phillip and N. Coltice "Temperature beneath continents as a function of continental cover and convective wavelength," J. Geophys. Res. **115**, B04408, doi:10.1029/2009JB006600 (2010).

[6]J-Q. Zhong, and J. Zhang, "Modeling the dynamics of a free boundary on turbulent thermal convection," Phys. Rev. E. **76**, 1 (2007).

[7]L. A Segel, "Nonlinear hydrodynamic stability theory and its applications to thermal convection and curved flows," in *Non-Equilibrium thermodynamics, Variational techniques, and stability*, edited by R. J. Donnelly and I. Prigogine (University of Chicago Press, Chicago, IL, 1966).

[8]J. T Stuart, "Nonlinear stability theory," Ann. Rev. Fluid Mech. **3**, 347 (1971), E. Palm, "Nonlinear thermal convection," Ann. Rev. Fluid Mech. **7**, 39 (1975).

[9]P. J. Heron and J. P. Lowman, "The effects of supercontinent size and thermal insulation on the formation of mantle plumes," Tectonophysics **510**, 28 (2011).